



DØ Note 6470-CONF

## Study of double parton interactions in diphoton + dijet events in $p\bar{p}$ collisions at $\sqrt{s} = 1.96$ TeV

The DØ Collaboration

URL <http://www-d0.fnal.gov>

(Dated: July 22, 2015)

We use a sample of diphoton + dijet events corresponding to an integrated luminosity of  $8.7 \text{ fb}^{-1}$  collected by the D0 detector at the Fermilab Tevatron collider to study properties of events with double parton scattering in  $p\bar{p}$  collisions at  $\sqrt{s} = 1.96$  TeV. We describe the measurement of the double parton event fraction and the double parton effective cross section ( $\sigma_{\text{eff}}$ ), which is found to be  $\sigma_{\text{eff}} = 21.3 \pm 1.5$  (stat)  $\pm 5.7$  (syst) mb.

*Results for Summer 2015 Conferences*

## I. INTRODUCTION

Many features of high energy inelastic hadron collisions are directly dependent on the parton structure of hadrons, which is not yet completely understood at the theoretical and experimental levels. Studies of this structure generally rely on a theoretical model of inelastic scattering of high energy nucleons, where a single parton (quark or gluon) from one nucleon (or a lepton in DIS experiments) interacts with a single parton from another nucleon. In this approach, the other “spectator” partons, which do not take part in a hard  $2 \rightarrow 2$  parton collision, participate in the so-called “underlying event”.

Currently, the information regarding the abundance of double parton (DP) interactions comprising two separate hard parton scatterings within one encounter of the beam hadrons [1–10] is a subject of high interest, because the growing LHC luminosity allows an opportunity to search for signals from new physics for which the DP events constitute a significant background, especially in the multijet final state, for example, for such processes as the production of the Higgs and  $W$  bosons, with the Higgs boson decaying into a pair of  $b$  quarks [11].

Several relevant measurements have been already performed using hadron collisions at  $\sqrt{s} = 63$  GeV [12],  $\sqrt{s} = 630$  GeV [13],  $\sqrt{s} = 1.8$  TeV [14, 15],  $\sqrt{s} = 1.96$  TeV [16–19] and  $\sqrt{s} = 7$  TeV [20, 21]. The first three measurements utilize a four jet final state where the transverse momentum of the jets in each jet pair is balanced, with the jets produced at almost opposite azimuthal angles. The studies are performed on samples corresponding to integrated luminosities of  $10 \text{ pb}^{-1}$ ,  $7.6 \text{ pb}^{-1}$ , and  $325 \text{ nb}^{-1}$ , respectively. AFS [12] has found (for jet transverse energy  $E_T^{jet} > 4$  GeV and pseudorapidity [22]  $|\eta^{jet}| \leq 1$ ) the ratio of DP/2jet cross sections to be  $6\% \pm 1.5\%(\text{stat.}) \pm 2.2\%(\text{syst.})$ . UA2 [13] retained only jet clusters with transverse momentum  $p_T^{jet} > 15$  GeV and within the range  $|\eta^{jet}| < 2$  and has set a 95% CL limit on the value of the DP cross-section  $\sigma_{DP} \leq 0.82 \text{ nb}$ . The first CDF measurement of the DP fraction in four jet events [14] found the DP cross section at the level of  $\sigma_{DP} = 63_{-28}^{+32} \text{ nb}$  for jets having  $p_T^{jet} \geq 25$  GeV and  $|\eta^{jet}| \leq 3.5$ . The CDF and D0 measurements [15, 16, 18] are based on the DP process comprising two parton scatterings with one of them having a dijet final state and the other having a  $\gamma$ +jet or  $\gamma$ +b(c)-jet final state.

As shown experimentally in Refs. [14–16] and described in Ref. [23], the substitution of one of the two dijet parton processes by a photon-jet or a diphoton process leads to about an order of magnitude increase in the ratio of the DP cross section to the cross section of the single parton (SP) scattering for the production of the same final state. This improves the ability to characterize the DP contribution in the data. Additionally, a technique for extracting an important physical parameter  $\sigma_{\text{eff}}$  has been proposed [15]. This method operates only on the quantities estimated from data analysis and minimizes theoretical assumptions that were used in the previous experiments.

The parameter  $\sigma_{\text{eff}}$  is related to the distance between partons in the nucleon [2, 3, 5, 12–15]:

$$\sigma_{\text{eff}}^{-1} = \int d^2\beta [F(\beta)]^2 \quad (1)$$

with  $F(\beta) = \int f(b)f(b-\beta)d^2b$ , where  $\beta$  is the impact parameter of the two colliding hadrons, and  $f(b)$  is a function describing the transverse spatial distribution of the partonic matter inside a hadron [5, 6]. The  $f(b)$  may depend on the parton flavor. The cross section for double parton scattering,  $\sigma_{DP}$ , is related to  $\sigma_{\text{eff}}$  [13–15] for 2- $\gamma$  and 2-jet process as:

$$\sigma_{DP} \equiv \frac{m}{2} \frac{\sigma^{\gamma\gamma} \sigma^{jj}}{\sigma_{\text{eff}}}. \quad (2)$$

The factor of  $1/2$  is due to the assumption that the probability of multiple parton interactions inside the proton follows a Poisson distribution [4]. For this analysis, the factor  $m$  is equal to 2 because the diphoton and double jet production processes are distinguishable (in the case of 4-jet production, i.e. two dijet processes,  $m = 1$ ).

Table I summarizes the available data on the measurements of  $\sigma_{\text{eff}}$ . The goal of our study is to obtain the DP rate and the effective cross section in the diphoton+dijet final state.

The main contributions to diphoton production at the Tevatron are from the  $q\bar{q} \rightarrow \gamma\gamma$  (Born) and  $gg \rightarrow \gamma\gamma$  (box) subprocesses, as well as from bremsstrahlung processes with single and double parton-to-photon fragmentations. Figure 1 shows representative Feynman diagrams of DP diphoton and dijet scattering. For dijet scattering the  $gg \rightarrow gg$  process is shown, as it is dominant in the jet kinematic range studied in this analysis.

Figure 2 shows the relative fraction of  $gg \rightarrow \gamma\gamma$  contribution to the total cross section, which is a combination of  $q\bar{q} \rightarrow \gamma\gamma$  and  $gg \rightarrow \gamma\gamma$  processes. For this analysis, which restricts jet momenta to the range of 15–40 GeV, the Born scattering significantly dominates the box process, with its fraction of about 70–80%. This analysis is based on a data sample collected by the D0 experiment between June 2006 and September 2011 using  $p\bar{p}$  collisions at  $\sqrt{s} = 1.96$  TeV corresponding to an integrated luminosity of  $8.7 \text{ fb}^{-1}$ .

TABLE I: Summary of the results, experimental parameters, and event selection criteria for the double parton analyses performed by the AFS, UA2, CDF, D0, ATLAS, and CMS Collaborations (no uncertainties are available for the AFS result).

	$\sqrt{s}$ (GeV)	final state	$p_T^{min}$ (GeV/c)	$\eta$ range	Result
AFS, 1986	63	$4jets$	$p_T^{jet} > 4$	$ \eta^{jet}  < 1$	$\sigma_{eff} \sim 5$ mb
UA2, 1991	630	$4jets$	$p_T^{jet} > 15$	$ \eta^{jet}  < 2$	$\sigma_{eff} > 8.3$ mb (95% C.L.)
CDF, 1993	1800	$4jets$	$p_T^{jet} > 25$	$ \eta^{jet}  < 3.5$	$\sigma_{eff} = 12.1^{+10.7}_{-5.4}$ mb
CDF, 1997	1800	$\gamma + 3jets$	$p_T^{jet} > 6$ $p_T^\gamma > 16$	$ \eta^{jet}  < 3.5$ $ \eta^\gamma  < 0.9$	$\sigma_{eff} = 14.5 \pm 1.7^{+1.7}_{-2.3}$ mb
D0, 2009	1960	$\gamma + 3jets$	$60 < p_T^\gamma < 80$	$ \eta^\gamma  < 1.0$ $1.5 <  \eta^\gamma  < 2.5$	$\sigma_{eff} = 16.4 \pm 2.3$ mb
ATLAS, 2013	7000	$W + 2jets$	$p_T^{jet} > 20$	$ \eta^{jet}  < 2.8$	$\sigma_{eff} = 15 \pm 3^{+5}_{-3}$ mb
CMS, 2014	7000	$W + 2jets$	$p_T^{jet} > 20$	$ \eta^{jet}  < 2.0$	$\sigma_{eff} = 20.7 \pm 6.6$ mb
D0, 2014	1960	$\gamma + 3jets$	$p_T^\gamma > 26$	$ \eta^\gamma  < 1.0$ $1.5 <  \eta^\gamma  < 2.5$	$\sigma_{eff} = 12.7 \pm 1.3$ mb
D0, 2014	1960	$\gamma + b/cjet + 2jets$	$p_T^\gamma > 26$	$ \eta^\gamma  < 1.0$ $1.5 <  \eta^\gamma  < 2.5$	$\sigma_{eff} = 14.6 \pm 3.3$ mb
D0, 2014	1960	$J/\psi J/\psi$			$\sigma_{eff} = 4.8 \pm 2.5$ mb

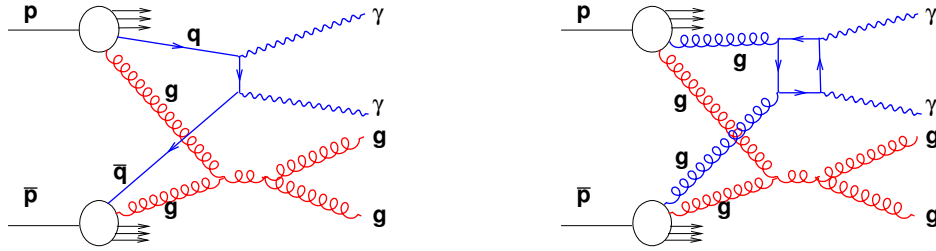


FIG. 1: (color online) Schematic view of DP scattering processes producing  $\gamma\gamma + \text{dijet}$  final state, Born-type process (left, blue) and box diagram (right, blue). The additional dijet scattering is shown in red.

The outline of the paper is as follows. Section II briefly describes the method for extracting  $\sigma_{eff}$  proposed in Ref. [15]. Section III introduces the D0 detector and data samples. Section IV includes the description of signal and background models used in this measurement. Section V describes the discriminating variable used to identify a data sample with an enhanced population of DP events. The procedure of finding the fraction of DP events is given in Section VI A. Section VI B contains a description of the analogous procedure used to measure the fraction of events with double  $p\bar{p}$  interactions. A summary of the efficiencies calculated in the measurement is presented in Section VII. In Section VIII, we calculate the effective cross section  $\sigma_{eff}$  for the diphoton+dijet final state. Conclusions and outlook are presented in Section IX.

## II. TECHNIQUE FOR EXTRACTING $\sigma_{eff}$ FROM DATA

The technique for extracting  $\sigma_{eff}$  has been used in a number of earlier measurements [15, 16, 18]. To avoid using theoretical predictions of the diphoton and dijet cross sections, the technique is based on a comparison of the number of  $\gamma\gamma + \text{dijet}$  events produced in DP interactions in single  $p\bar{p}$  collisions to the number of  $\gamma\gamma + \text{dijet}$  events produced in two separate  $p\bar{p}$  collisions. In the latter class of events, referred to as double interaction (DI) events, two hard parton interactions occur in exactly two separate  $p\bar{p}$  collisions within the same beam crossing. The parton scatterings in the DP events are assumed to be uncorrelated [1–5].

The single [24] and double [25] diffractive processes contribute just about 1% to the total dijet production cross

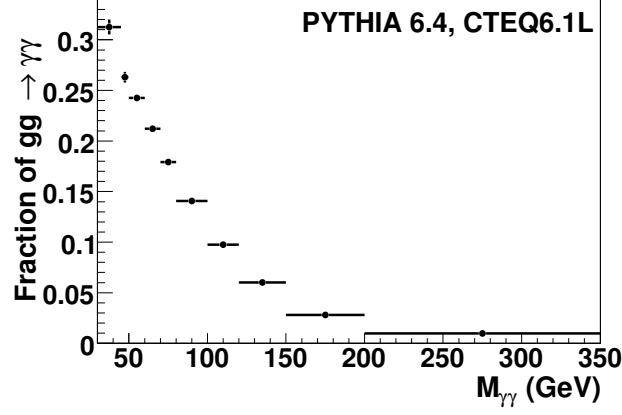


FIG. 2: Fraction of  $gg \rightarrow \gamma\gamma$  contribution to the total direct cross section caused by  $q\bar{q} \rightarrow \gamma\gamma$  and  $gg \rightarrow \gamma\gamma$  processes.

section with jet  $p_T \gtrsim 15$  GeV. Therefore the diphoton and dijet events are produced mainly as a result of an inelastic non-diffractive (hard)  $p\bar{p}$  interactions. In a  $p\bar{p}$  beam crossing with two inelastic non-diffractive collisions the probability for a DI event is

$$P_{\text{DI}} = 2 \frac{\sigma^{\gamma\gamma}}{\sigma_{\text{hard}}} \frac{\sigma^{jj}}{\sigma_{\text{hard}}}, \quad (3)$$

where  $\sigma^{\gamma\gamma}/\sigma_{\text{hard}}$  ( $\sigma^{jj}/\sigma_{\text{hard}}$ ) is the probability for producing a diphoton (dijet) event satisfying particular jet (and photon) selection criteria in two separate hard processes and  $\sigma_{\text{hard}}$  is the cross section of the hard  $p\bar{p}$  interactions. The factor of 2 accounts for the fact that the two scatterings (producing diphoton and dijet events) can be ordered in two ways with respect to the two collision vertices. The number of DI events can be obtained from  $P_{\text{DI}}$ , after correcting for geometric and kinematic acceptance  $A_{\text{DI}}$ , selection efficiency (including trigger efficiency)  $\epsilon_{\text{DI}}$ , and the two-vertex selection efficiency  $\epsilon_{2\text{vtx}}$ , and also multiplied by the number of beam crossings with exactly two hard collisions  $N_c(2)$  (modified by the probability to reconstruct two  $p\bar{p}$  vertices):

$$N_{\text{DI}} = 2 \frac{\sigma^{\gamma\gamma}}{\sigma_{\text{hard}}} \frac{\sigma^{jj}}{\sigma_{\text{hard}}} N_c(2) A_{\text{DI}} \epsilon_{\text{DI}} \epsilon_{2\text{vtx}}. \quad (4)$$

Similarly to  $P_{\text{DI}}$ , the probability for DP events,  $P_{\text{DP}}$ , given a beam crossing with one hard collision (modified by the probability to reconstruct one  $p\bar{p}$  vertex) is

$$P_{\text{DP}} = \frac{\sigma^{\text{DP}}}{\sigma_{\text{hard}}} = \frac{\sigma^{\gamma\gamma}}{\sigma_{\text{eff}}} \frac{\sigma^{jj}}{\sigma_{\text{hard}}}, \quad (5)$$

where we used Eq. (2). The number of DP events,  $N_{\text{DP}}$ , can be expressed as  $P_{\text{DP}}$  corrected for the acceptance,  $A_{\text{DP}}$ , selection efficiency (including trigger efficiency)  $\epsilon_{\text{DP}}$ , and the single vertex selection efficiency,  $\epsilon_{1\text{vtx}}$  multiplied by the number of beam crossings with exactly one hard collision  $N_c(1)$ :

$$N_{\text{DP}} = \frac{\sigma^{\gamma\gamma}}{\sigma_{\text{eff}}} \frac{\sigma^{jj}}{\sigma_{\text{hard}}} N_c(1) A_{\text{DP}} \epsilon_{\text{DP}} \epsilon_{1\text{vtx}}. \quad (6)$$

The numbers of DI (DP) events  $N_{\text{DI}}$  ( $N_{\text{DP}}$ ) can be determined from the number of two(one)-vertex  $\gamma\gamma$ +dijet events  $N_{1\text{vtx}}$  ( $N_{2\text{vtx}}$ ) as  $N_{\text{DI}} = f_{\text{DI}} P_{\text{DI}}^{\gamma\gamma} N_{2\text{vtx}}$  ( $N_{\text{DP}} = f_{\text{DP}} P_{\text{DP}}^{\gamma\gamma} N_{1\text{vtx}}$ ), where  $f_{\text{DI}}$  ( $f_{\text{DP}}$ ) and  $P_{\text{DI}}^{\gamma\gamma}$  ( $P_{\text{DP}}^{\gamma\gamma}$ ) are the fraction of DI (DP) events and diphoton purity in the two(one)-vertex dataset, respectively.  $f_{\text{DP}}$  is estimated from the dataset with one  $p\bar{p}$  collision using a template fitting method, while  $f_{\text{DI}}$  can be found from data events with two  $p\bar{p}$  collisions using a jet-track algorithm. The complete description of the techniques used for  $f_{\text{DP}}$  and  $f_{\text{DI}}$  estimates are described in Sections VIA and VIB and diphoton purity in Sec. VII A.

Using the ratio  $N_{\text{DI}}/N_{\text{DP}}$  allows one to obtain the expression for  $\sigma_{\text{eff}}$ :

$$\sigma_{\text{eff}} = \frac{N_{\text{DI}}}{N_{\text{DP}}} \frac{A_{\text{DP}}}{A_{\text{DI}}} \frac{\epsilon_{\text{DP}}}{\epsilon_{\text{DI}}} \frac{\epsilon_{1\text{vtx}}}{\epsilon_{2\text{vtx}}} R_c \sigma_{\text{hard}}, \quad (7)$$

where  $R_c = N_c(1)/2N_c(2)$ .

It is worth noting that: (a)  $\sigma^{\gamma\gamma}$  and  $\sigma^{jj}$  cross sections cancel in this ratio; and (b) the remaining efficiencies and acceptances for DP and DI events enter only as ratios (i.e. all common uncertainties are reduced as well). To calculate those efficiencies, acceptances, and their ratios, we used the data based models which are described in Section IV A.

The main background for the DP events is due to a contribution from the SP scattering processes,  $q\bar{q} \rightarrow \gamma\gamma gg$  and  $gg \rightarrow \gamma\gamma gg$ . These processes are caused by gluon radiation in the initial or the final state, and can also result from photon fragmentation events.

### III. D0 DETECTOR AND DATA SAMPLES

The D0 detector is described in detail in Refs. [26–28]. Photon candidates are identified as isolated clusters of energy depositions in one of three uranium and liquid argon sampling calorimeters. The central calorimeter (CC) covers the pseudorapidity range  $|\eta_{\text{det}}| < 1.1$ , and the two end calorimeters cover up to  $|\eta_{\text{det}}| \approx 4.2$ . In addition, the plastic scintillator intercryostat detector covers the region  $1.1 < |\eta_{\text{det}}| < 1.4$ . The electromagnetic (EM) section of the calorimeter is segmented longitudinally into four layers and transversely into cells in pseudorapidity and azimuthal angle  $\Delta\eta_{\text{det}} \times \Delta\phi_{\text{det}} = 0.1 \times 0.1$  ( $0.05 \times 0.05$  in the third layer of the EM calorimeter). The hadronic portion of the calorimeter is located behind the EM section. The calorimeter surrounds a tracking system consisting of a silicon microstrip tracking (SMT) detector and scintillating fiber tracker, both located within a 1.9 T solenoidal magnetic field. The solenoid magnet is surrounded by the central preshower (CPS) detector located immediately before the calorimeter. The CPS consists of approximately one radiation length of lead absorber surrounded by three layers of scintillating strips. The luminosity of colliding beams is measured using plastic scintillator arrays installed in front of the two end calorimeter cryostats [29].

The current measurement is based on  $8.7 \text{ fb}^{-1}$  of data collected after the D0 detector upgrade in 2006 [28], while the previous measurements [16, 17] were made using the data collected before this upgrade. The events used in this analysis pass the triggers designed to identify high- $p_T$  clusters in the EM calorimeter with loose shower shape requirements for photons. These triggers have  $\approx 96\%$  efficiency at the photon transverse momentum  $p_T^\gamma \approx 30 \text{ GeV}$  and are 100% efficient for  $p_T^\gamma > 35 \text{ GeV}$ .

To select photon candidates in our data samples, we use the following criteria [30, 31]: EM objects are reconstructed using a simple cone algorithm with a cone size of  $\Delta\mathcal{R} = \sqrt{(\Delta\eta)^2 + (\Delta\phi)^2} = 0.2$ . Regions with poor photon identification and degraded  $p_T^\gamma$  resolution at the boundaries between calorimeter modules and between the central and endcap calorimeters are excluded from the analysis. Each photon candidate is required to deposit more than 96% of the detected energy in the EM section of the calorimeter and to be isolated in the angular region between  $\Delta\mathcal{R} = 0.2$  and  $\Delta\mathcal{R} = 0.4$  around the center of the cluster:  $(E_{\text{tot}}^{\text{iso}} - E_{\text{core}}^{\text{iso}})/E_{\text{core}}^{\text{iso}} < 0.07$ , where  $E_{\text{tot}}^{\text{iso}}$  is the total (EM+hadronic) tower energy in the  $(\eta, \phi)$  cone of radius  $\Delta\mathcal{R} = 0.4$  and  $E_{\text{core}}^{\text{iso}}$  is EM energy within a radius of  $\Delta\mathcal{R} = 0.2$ . Candidate EM clusters that match to a reconstructed track are excluded from the analysis. We also require the energy-weighted EM cluster width in the finely-segmented third EM layer to be consistent with that expected for a photon-initiated electromagnetic shower. In addition to the calorimeter isolation cut, we also apply a track isolation cut, requiring the scalar sum of the track transverse momenta in an annulus  $0.05 \leq \Delta\mathcal{R} \leq 0.4$  to be less than 1.5 GeV. To further suppress the jet background, the photons are selected to satisfy the same requirement on the neural network (NN) discriminant as in [32].

Jets are reconstructed using an iterative midpoint cone algorithm [33] with a cone size of 0.7. Jets must satisfy quality criteria that suppress background from leptons, photons, and detector noise effects. Jet transverse momenta are corrected to the particle level [34].

Two photons must be separated from each other by  $\Delta\mathcal{R} > 0.4$  and from each jet by  $\Delta\mathcal{R} > 0.9$ . Jets must be separated from each other by  $\Delta\mathcal{R} > 1.4$ . Each event must contain at least two photons in the pseudorapidity region  $|\eta^\gamma| < 1.0$  and at least two jets with  $|\eta^{\text{jet}}| < 3.5$ . The photon with the highest  $p_T$  is named the “leading photon,” or first photon, and the photon with the second highest  $p_T$  is denoted as the second photon. Similar terminology is applied to the jets. Events are selected with the leading photon transverse momentum  $p_T^\gamma > 16 \text{ GeV}$ , the second photon  $p_T^\gamma > 15 \text{ GeV}$ , and jets satisfying  $15 < p_T^{\text{jet}} < 40 \text{ GeV}$ . The upper requirement on the  $p_T$  of the jets increases the fraction of DP events in the sample [16]. The numbers of events with a exactly one identified  $p\bar{p}$  collision (1VTX), exactly two identified  $p\bar{p}$  collisions (2VTX), and their ratio are shown in Table II.

### IV. DATA, SIGNAL, AND BACKGROUND EVENT MODELS

This section presents an overview of the DP and DI models built using data and MC samples to estimate the number of DP and DI events in data,  $N_{\text{DP}}$  and  $N_{\text{DI}}$ . These models are also used to estimate the selection efficiencies

TABLE II: The number of selected  $\gamma\gamma$  + dijet events with a single  $p\bar{p}$  collision ( $N_{1vtx}$ ), two  $p\bar{p}$  collisions ( $N_{2vtx}$ ), and their ratio.

$N_{1vtx}$	$N_{2vtx}$	$N_{2vtx}/N_{1vtx}$
401	442	1.102

and geometric and kinematic acceptances for DP and DI events.

### A. Signal models

Because  $\sigma_{\text{eff}}$  depends on DP and DI events as shown in Eq. 7, both classes of events are considered signal events.

- **DP data event model (MIXDP):**

The DP event model is constructed by overlaying one event from an inclusive data sample of  $\gamma\gamma$  data events with another event from a sample of inelastic non-diffractive events selected with a zero or minimum bias trigger (a trigger that only requires hits in the luminosity detectors) and a requirement of at least one reconstructed jet (“MB” sample) [16, 34]. Both input samples contain events with exactly one reconstructed  $p\bar{p}$  collision vertex. The resulting mixed event is required to satisfy the same selection criteria as applied to  $\gamma\gamma$  + dijet data events with a single  $p\bar{p}$  collision. The MIXDP sample provides independent parton scatterings with  $\gamma\gamma$  and dijet final states, by construction. Because the  $\gamma\gamma$  process in a DP event is dominated by small parton momentum fractions ( $x$ ), the  $x$  values in the dijet production process remaining after the first parton interaction occurs are generally unaffected, i.e. the two interactions have negligible correlation in the momentum space. Two possible event configurations with the  $\gamma\gamma$  + dijet final state in a single  $p\bar{p}$  collision are shown in Fig. 3.

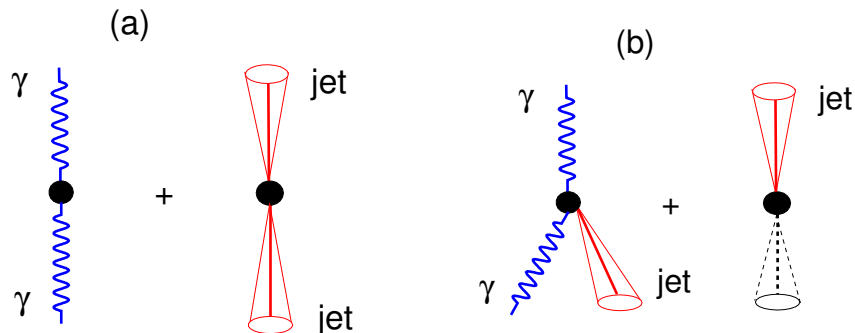


FIG. 3: (color online) Diagrams of  $\gamma\gamma$  + dijet final state in the events with a single  $p\bar{p}$  collision. (a): DP scattering with diphoton production overlaid with dijet production; (b): DP scattering with diphoton +1 jet production overlaid with dijet production, in which one of the two jets is lost (dotted line). They can also be used as an illustration of the two DI events if one assumes that the processes shown come from two distinct  $p\bar{p}$  collisions.

- **DI data event model (MIXDI):**

The  $\gamma\gamma$  + dijet DI signal event model is built from an overlay of  $\gamma\gamma$  and MB events with  $\geq 1$  selected jets. This is prepared similarly to MIXDP sample with the requirement of exactly two reconstructed  $p\bar{p}$  collision vertices in both data samples instead of one such vertex in the samples used for MIXDP. Thus, the second  $p\bar{p}$  collision contains only soft underlying energy that can contribute energy to a jet cone, or a photon isolation cone. In addition, in the case of jets in MB component of the MIXDI mixture, if there are more than one jet, both jets are required to originate from the same vertex, using jet track information, as discussed in Appendix B of Ref. [16]. The resulting  $\gamma\gamma$  + dijet events undergo the same selection as applied to the data sample with two  $p\bar{p}$  collision vertices.

- **DP and DI MC models (MCDP and MCDI):**

To create signal MC models for DP and DI events, we use an overlay of MC  $\gamma\gamma$  and dijet events. These events are generated with SHERPA [35] and PYTHIA [36] event generators, respectively, and are processed by a GEANT-based [37] simulation of the D0 detector response. To accurately model the effects of multiple  $p\bar{p}$  interactions

and detector noise, data events from random  $p\bar{p}$  crossings are overlaid on the MC events using data from the same data taking period as considered in the analysis. These MC events are then processed using the same reconstruction code as for data. We also apply additional smearing to the reconstructed photon and jet  $p_T$  so that the measurement resolutions in MC match those in data. These MC events are used to create single- and two-vertex samples.

Using the  $\gamma\gamma$  and dijet MC samples, we create  $\gamma\gamma$  + dijet DP and DI MC models, similarly to those constructed for MIXDP and MIXDI data samples, i.e. with only one and only two reconstructed primary interaction vertexes, respectively, by examining information for jets and the photon at both the reconstructed and particle level. These samples are used to calculate efficiencies and acceptances for DP and DI events. As a cross check, we have compared  $p_T$  and  $\eta$  distributions of the jets and photons at the reconstructed level in these models with those in the MIXDP and MIXDI data samples. Small discrepancies have been resolved by reweighting these MC spectra and creating models denoted as data-like MCDP and MCDI.

## B. Background model

To extract the DP signal from data, we need to subtract  $\gamma\gamma$ +dijet single parton (SP) background.

### • SP one-vertex event model (SP1VTX):

A background to the DP events are single parton-parton scatters with two additional bremsstrahlung jets resulting in a  $\gamma\gamma$  + dijet final state in a single  $p\bar{p}$  collision event. To model this background, we consider a sample of MC  $\gamma\gamma$  + dijet events generated with PYTHIA and SHERPA with no multiple parton interaction (MPI) modeling. The SP1VTX sample contains the final state with two photons and two additional bremsstrahlung jets with the same selection criteria as applied to the data sample with a single  $p\bar{p}$  collision vertex. The SHERPA SP model is taken as the default.

## V. DISCRIMINATING VARIABLE

A DP event contains two independent  $2 \rightarrow 2$  parton-parton scatterings within the same  $p\bar{p}$  collision. The same final state can be produced by the SP  $2 \rightarrow 4$  process, resulting in  $\gamma\gamma$  and two bremsstrahlung jets with substantially different kinematic distributions. Discrimination between these processes is obtained by examining the azimuthal angle between the  $p_T$  imbalance vectors of photon and jet pairs in  $\gamma\gamma$  + dijet events,

$$\Delta S \equiv \Delta\phi(\vec{q}_T^1, \vec{q}_T^2), \quad (8)$$

where  $\vec{q}_T^1 = \vec{p}_T^{\gamma 1} + \vec{p}_T^{\gamma 2}$  and  $\vec{q}_T^2 = \vec{p}_T^{\text{jet}1} + \vec{p}_T^{\text{jet}2}$ . Figure 4 illustrates the orientation of photons and jets transverse momentum vectors in  $\gamma\gamma$  + dijet events, as well as the imbalance vectors  $\vec{q}_T^1$  and  $\vec{q}_T^2$ .

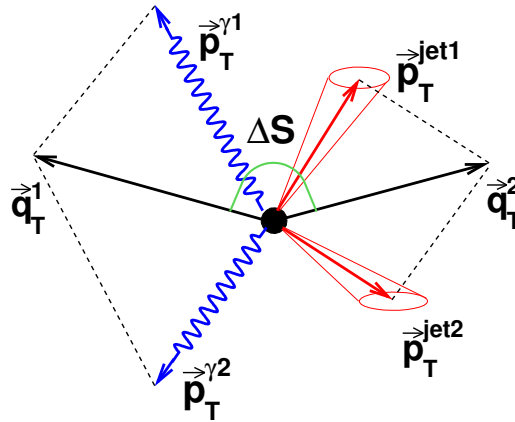


FIG. 4: (color online) A diagram illustrating the orientation of photon and jet transverse momenta vectors in  $\gamma\gamma$  + dijet events. Vectors  $\vec{q}_T^1$  and  $\vec{q}_T^2$  are the  $p_T$  imbalance vectors of diphoton and dijet pairs, respectively.

For DP events, where the photons come from one parton-parton scattering and the two jets come from another parton-parton scattering, the  $\Delta S$  angle is arbitrary. However, there is a tendency to produce events towards  $\Delta S = \pi$  caused by the DP events with an additional bremsstrahlung jet in the first parton-parton scattering shown on Fig. 3(b). Momentum conservation in the initial state gluon radiation causes  $\Delta S$  to peak strongly near  $\pi$  in SP, but detector resolution effects and additional gluon radiation produce a tail extending to smaller angles.

## VI. FRACTIONS OF DP AND DI EVENTS

### A. Fractions of DP events

In order to calculate  $\sigma_{\text{eff}}$ , one needs to measure the number of DP events ( $N_{\text{DP}}$ ) which enters Eq. (7), as the product of the fraction of DP events ( $f_{\text{DP}}$ ) in the 1VTX data sample times the size of the 1VTX sample. The fraction is estimated in  $\gamma\gamma$  + dijet 1VTX data sample using the MIXDP and the SP1VTX models described in Section IV.

The measurement of  $f_{\text{DP}}$  (and then the effective cross section) is done by using the DP and SP templates of the discriminating variable  $\Delta S$ . In each segment of the  $\Delta S$  data can be represented by the sum of the two templates weighted by their event fractions,  $\text{DATA} = f_{\text{DP}} \text{MIXDP} + (1 - f_{\text{DP}}) \text{SP1VTX}$ . To derive this formula, we assume equally normalized DATA, MIXDP, and SP1VTX distributions. If we introduce the fractions  $\epsilon_{\text{DATA}}$ ,  $\epsilon_{\text{MIXDP}}$ ,  $\epsilon_{\text{SP}}$  of all selected events passing a specific  $\Delta S < \Delta S_{\text{cut}}$  cut in data, DP signal, and SP background, respectively, we can invert this formula to extract  $f_{\text{DP}}$ :

$$f_{\text{DP}} = \frac{\epsilon_{\text{DATA}} - \epsilon_{\text{SP}}}{\epsilon_{\text{MIXDP}} - \epsilon_{\text{SP}}} \quad (9)$$

Equation (10) shows the value found by averaging  $f_{\text{DP}}$  over various cuts on  $\Delta S$  set using the covariance matrix of the measurements, which was found close to the one for  $\Delta S < 2.5$  cut.

$$f_{\text{DP}}^{\text{ave}} = 0.193 \pm 0.037 \quad (10)$$

As a cross check, the fraction  $f_{\text{DP}}$  is found using a maximum likelihood fit [38] of the  $\Delta S$  distribution of the data to signal and background templates that are taken to be the shapes of the  $\Delta S$  distribution in the MIXDP and SP1VTX models, respectively. Signal and background models are described in Section IV and undergo all the selection criteria applied to the data sample, except for the NN requirement, to increase the data statistics, which does not alter the  $\Delta S$  shape. Events generated with SHERPA with no MPI modeling are used as a SP1VTX model. The result of the fit is shown in Fig. 5. The DP fraction found from the fit is:

$$f_{\text{DP}}^{\text{fit}} = 0.191 \pm 0.067 \quad (11)$$

The DP event fractions found using the two different methods agree within uncertainties. Since the fitting method has larger uncertainty we take the  $f_{\text{DP}}$  found using the efficiency method as a central value, and the difference between them as systematic uncertainty.

### B. Fractions of DI events

The fraction of events with two  $p\bar{p}$  collisions,  $f_{\text{DI}}$ , within the same bunch crossing is determined using a discriminant constructed from the reconstructed track information of a jet and the assignment of tracks to the two  $p\bar{p}$  collision vertices (PV0 and PV1). We use the  $p_T$ -weighted position along the beam ( $z$ ) axis of all tracks associated to the jet and the fraction of charged particles in the jet (CPF). The CPF discriminant is based on the fraction of total charged particles' transverse momentum (i.e., total track  $p_T$ ) in each jet  $i$  originating from each identified vertex  $j$  in the event:

$$\text{CPF}(\text{jet}_i, \text{vtx}_j) = \frac{\sum_k p_T(\text{trk}_k^{\text{jet}_i}, \text{vtx}_j)}{\sum_n \sum_l p_T(\text{trk}_l^{\text{jet}_i}, \text{vtx}_n)}, \quad (12)$$

where the sum is taken over tracks within the jet cone in the numerator and also over all vertices in the denominator. Each jet is required to have  $\text{CPF} > 0.5$  and at least two tracks. Each jet is assigned to a  $p\bar{p}$  vertex based on the tracking information. In events with two  $p\bar{p}$  collisions, jets in  $\gamma\gamma$  + dijet events may originate either from the best primary vertex (PV0) or next-to-the-best vertex (PV1). Therefore we can define three classes of events:

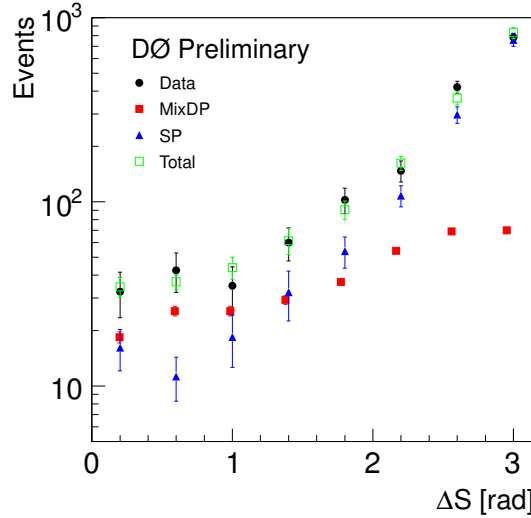


FIG. 5: The fit of the data  $\Delta S$  distribution with SP and DP templates to data to extract the DP fraction. No NN selection requirement is applied. Relaxing the NN selection requirement does not alter the shapes of the distributions. The black points correspond to data, red boxes to the DP signal MIXDP model normalized to the  $f_{\text{DP}}$  fraction obtained from the fit, and the blue triangles are the SP background template (SP1VTX) normalized to its fraction ( $1 - f_{\text{DP}}$ ). The green open boxes correspond to the sum of the signal and background (Total).

I: Both jets originate from PV0;

II: One jet originates from PV0 and one jet from PV1;

III: Both jets originate from PV1;

Class I corresponds to a type of  $\gamma\gamma$  + dijet events where both jets originate from the same  $p\bar{p}$  collision with no jet activity in the other one, i.e. to background (non-DI) events. Classes II and III correspond to  $\gamma\gamma$  + dijet events with at least one jet (Jet1 or Jet2) coming from PV1.

A jet-to-vertex matching procedure is used for  $f_{\text{DI}}$  extraction which depends on the resolution of a jet assignment to a vertex. This resolution can be calculated in the  $\gamma$  + jet data event sample with a single  $p\bar{p}$  collision. Since these events have only one reconstructed  $p\bar{p}$  vertex all the jets should originate from this vertex. By measuring the distance between the jet origin position along the z-axis and the  $p\bar{p}$  vertex position, one can estimate the resolution of the jet vertexing algorithm, which is found to be approximately a Gaussian with  $\sigma_z \approx 1.2$  cm. In this analysis we require all jets to point to a vertex within  $3\sigma_z$ . The DI event fraction is obtained as the ratio of the numbers of events in classes II and III together and in the whole sample and is found to be  $f_{\text{DI}} = 0.193 \pm 0.021$ .

A distance along the z-axis between the two vertices can affect the DI fraction. To study this effect, a distance between the two vertices is varied up to  $7\sigma_z$  and the DI fraction is extracted with the requirement above. Table III shows  $f_{\text{DI}}$  with respect to the distance between two vertices,  $\Delta Z(PV0, PV1)$ . The difference between the default  $f_{\text{DI}}$  value and  $f_{\text{DI}}$  found when the distance between the two vertices is greater than  $7\sigma_z$  is taken as a systematic uncertainty.

TABLE III: DI event fraction with respect to  $\Delta Z(PV0, PV1)$

$\Delta Z(PV0, PV1)$	
Default	$0.193 \pm 0.021$
$> 3\sigma_z$	$0.195 \pm 0.021$
$> 5\sigma_z$	$0.200 \pm 0.022$
$> 7\sigma_z$	$0.203 \pm 0.023$

Finally, the fraction extracted is:

$$f_{\text{DI}} = 0.193 \pm 0.021 \text{ (stat)} \pm 0.010 \text{ (syst)} \quad (13)$$

In the selection of 2VTX events, we did not use the information about the photon original vertex. The fact that one or both photons may not come from PV0 introduces an uncertainty which we estimate by comparing the resolution of the  $z$ -position of the photon original vertex for 1VTX and 2VTX cases. We study the events with a photon EM cluster in the CC region with a matched CPS 3D cluster. These events provide a directional extrapolation of the photon and allow a determination of its position at the  $z$ -axis. We consider samples with at least one CPS 3D cluster matched to the photon EM cluster. The fraction of events in 2VTX SHERPA and PYTHIA MC samples when both photons and both jets come from PV1 is found to be about 7%. The amount of background due to events having a photon-jet in each of the two vertexes in the 2VTX case or due to DP photon-jet events in the 1VTX case is estimated using the inclusive photon-jet sample from [30] correcting for the difference in fiducial selections. It is estimated to be less than 2% of the number of signal  $\gamma\gamma$  + dijet events or 0.5% of the number of DI events. These numbers are included into the systematic uncertainty on the DP and DI event fractions, respectively.

## VII. DP AND DI EFFICIENCIES, $R_c$ AND $\sigma_{\text{hard}}$

### A. Ratio of photon purity in DP and DI events

There are two major sources of background events to direct diphoton production: (i) Drell-Yan events with both electrons misidentified as photons due to tracking inefficiency, and (ii)  $\gamma$  + jet and dijet events with jet(s) misidentified as photon(s) [32]. The  $W$  +  $jet/\gamma$  background with  $W \rightarrow e\nu$  decay has been estimated from MC and found to be negligible.

We use  $Z/\gamma^* \rightarrow ee$  PYTHIA+ALPGEN MC samples to estimate Drell-Yan contribution. The next-to-next-to-leading-order (NNLO)  $p\bar{p} \rightarrow Z/\gamma^* \rightarrow ee$  cross section [39] is used for the absolute normalization and the generator level  $Z/\gamma^*$  boson  $p_T$  has been re-weighted to the measured data distribution. The expected number of events from the Drell-Yan process is 2.19(0.5%) and 2.41(0.5%) in case of 1VTX and 2VTX events, respectively. The numbers in parentheses correspond to the percentage of the Drell-Yan contribution to the data sample.

To estimate the fraction of diphoton events, we use variables sensitive to the internal structure of the electromagnetic shower. The outputs of the photon artificial neural networks (ANN) for the photons in the central calorimeter, trained on MC samples with direct photons and dijets have been chosen as a discriminant between signal and background events. The signal MC and data events were preselected in order to satisfy the main photon and jets selection criteria described in Section III. Since the signal events cannot be identified on an event by event basis, their fraction (purity)  $P^{\gamma\gamma}$  is determined for a given  $p_T$  bin statistically. The photon purity is defined as the ratio

$$P^{\gamma\gamma} = \frac{N_{\text{data}} - N_{\text{non-}\gamma\gamma} - N_{\text{DY}}}{N_{\text{data}}}, \quad (14)$$

where  $N_{\text{non-}\gamma\gamma}$  ( $N_{\text{DY}}$ ) is the number of  $\gamma$  + jet and dijet (Drell-Yan) events and  $N_{\text{data}}$  is the number of events in data that satisfy the photon selection criteria.

The two-dimensional distribution of ANN outputs of the two photon candidates in data is fitted using two-dimensional ANN output templates of signal photons from SHERPA MC and templates of PYTHIA MC jet samples, where special requirements are applied at the generator level to enrich the sample with jets having an electromagnetic shower shape similar to that of the photon. The fit uses the same maximum likelihood method [38] as a cross check fit for  $f_{\text{DP}}$ , see Sec. VIA. The results of the diphoton purities in DP and DI events, and their ratio are presented in Table IV.

TABLE IV: Diphoton event purity in DP and DI events and their ratio

Sample	SHERPA	PYTHIA
$P_{\text{DP}}^{\gamma\gamma}$	$0.688 \pm 0.005$	$0.608 \pm 0.028$
$P_{\text{DI}}^{\gamma\gamma}$	$0.689 \pm 0.025$	$0.623 \pm 0.029$
$P_{\text{DI}}^{\gamma\gamma}/P_{\text{DP}}^{\gamma\gamma}$	$1.002 \pm 0.039$	$1.025 \pm 0.067$

We identify an additional source of systematic uncertainty due to model dependence as a half of the difference between the ratio of purities calculated using different signal models generated by PYTHIA and SHERPA. It is estimated to be 1.2%.

Another source of systematic uncertainty is due to the fragmentation model used in PYTHIA and caused by the uncertainty in the fragmentation functions  $D_{\pi,\eta}(z)$ . This uncertainty is estimated by varying the number of  $\pi^0$  and

$\eta$  mesons in the dijet sample by a factor of 2 and calculating the purity using the modified templates and is found to be equal to 3%.

### B. Ratio of geometric acceptances in DP and DI events

The acceptance ( $A$ ) is calculated as a ratio of  $N_i^{\text{reco}}/N_i^{\text{part}}$ , where  $N_i^{\text{reco}}$  and  $N_i^{\text{part}}$  are the numbers of events at the reconstruction and generator (true) level, respectively. It takes into account the events lost due to geometric and basic kinematic selection criteria which are aimed at keeping EM clusters reconstructed in the fiducial regions in  $\eta$  and  $\phi$  of the calorimeter (i.e. to avoid calorimeter section boundaries and edges) [26] and two jets, and corrects for the noise and the contribution from true events outside the fiducial region reconstructed inside the fiducial region and vice versa.

To estimate acceptances in one and two  $p\bar{p}$  collisions, we use the signal MCDP and MCDI samples described in Section IV. These samples mix diphoton events generated by SHERPA and dijet events generated by PYTHIA. The acceptance is calculated with respect to the following photon and jet selection criteria:

- Generator level:  $p_T^{\gamma_1} > 16$  GeV,  $p_T^{\gamma_2} > 15$  GeV,  $|\eta| < 1.0$ ;  
jets with  $15 < p_T^{\text{jet}1} \leq 40$  GeV and  $15 < p_T^{\text{jet}2} \leq 40$  GeV,  $|\eta| < 3.5$  ;
- Reconstruction level:  $p_T^{\gamma_1} > 16$  GeV,  $p_T^{\gamma_2} > 15$  GeV,  $|\eta| < 1.0$ ,  $|\eta^{\text{det}}| < 1.0$ ,  
 $\eta$  and  $\phi$  away from the calorimeter cell boundaries, fraction of the photon energy in the EM calorimeter greater than 0.9, calorimeter isolation requirement in the  $0.2 < \Delta R < 0.4$  annulus around the photon relaxed to 0.15;  
jets with  $15 < p_T^{\text{jet}} \leq 40$  GeV,  $|\eta| < 3.5$ .

In Table V, we present the photon and jet acceptance for 1VTX (MCDP) and 2VTX (MCDI) samples and their ratio. The difference between 1VTX and 2VTX acceptances is mostly caused by different amounts of underlying

TABLE V: Geometric acceptances in DP and DI events and their ratio.

$A_{DP}$	$A_{DI}$	$A_{DP}/A_{DI}$
$0.429 \pm 0.008$	$0.826 \pm 0.019$	$0.521 \pm 0.015$

energy falling inside the photon and jet cones resulting in different efficiencies for passing the photon and jet  $p_T$  requirements. The uncertainties due to JES, JER, and the model dependence of the individual acceptances largely cancel in the ratio.

### C. Ratio of photon efficiencies in DP and DI events

The DP and DI events differ from each other by the number of  $p\bar{p}$  collision vertices (one vs. two), and therefore their selection efficiencies  $\epsilon_{DP}$  and  $\epsilon_{DI}$  may differ due to different amounts of soft unclustered energy in the single and double  $p\bar{p}$  collision events. This could lead to different photon selection efficiencies because of different amounts of energy in the track and calorimeter isolation cones around the photon.

The efficiency for passing the photon selection criteria is estimated using  $\gamma\gamma$ +dijet PYTHIA and SHERPA MC events. The events are preselected with all jet cuts and loose photon identification cuts (which are used in the acceptance calculation) split into 1VTX and 2VTX samples. The trigger efficiency is applied to the event reconstruction level as in [32]. The efficiency is calculated from the ratio of the number of events that pass the photon selection criteria weighted by the trigger efficiency to the number of events that pass the preselection criteria. In Table VI, we present the photon efficiencies for DP and DI events. Uncertainties are due to limited MC statistics.

TABLE VI: Photon efficiencies in a single and double  $p\bar{p}$  collisions  $\gamma\gamma$  + dijet SHERPA and PYTHIA MC samples. Uncertainties are due to limited MC statistics.

Sample	SHERPA	PYTHIA
$\epsilon_{DP}$	$0.477 \pm 0.035$	$0.576 \pm 0.010$
$\epsilon_{DI}$	$0.333 \pm 0.021$	$0.419 \pm 0.009$
$\epsilon_{DP}/\epsilon_{DI}$	$1.434 \pm 0.138$	$1.372 \pm 0.039$

The difference in the efficiencies between PYTHIA and SHERPA is used as an estimate of the systematic uncertainty due to model dependence. The selection efficiencies for DP and DI events enter Eq. (7) only as ratios, substantially canceling correlated systematic uncertainties. The PYTHIA ratio, which has the smallest systematic uncertainty, is used in the  $\sigma_{\text{eff}}$  calculation.

#### D. Ratio of vertex efficiencies

A correction  $\epsilon_{1vtx}$  ( $\epsilon_{2vtx}$ ) is made for the events that are lost in the DP (DI) candidate sample due to the single (double) vertex requirement,  $|z| < 60$  cm and  $N_{trk} \geq 3$ . To calculate the efficiency for events with 1  $p\bar{p}$  collision to pass the vertex requirement we use  $\gamma\gamma$  + dijet data with photon and jet selection criteria. The efficiency to simultaneously satisfy the two-vertex requirement is estimated separately for each event type, since the vertex efficiency depends on the objects originating from the vertex. For Type I events, we calculate  $\epsilon_{2vtx}$  as a product of the efficiency to pass the vertex cuts in the diphoton 2VTX data sample and the efficiency to pass the vertex cuts for dijets in the 2VTX MB sample. Similarly, for Type II events we calculate the  $\epsilon_{2vtx}$  efficiency as a product of the efficiency to pass the vertex cuts for the  $\gamma\gamma$  + 1 jet 2VTX data sample and the efficiency to pass the vertex cuts for jets in the 2VTX min-bias sample. Final efficiency is a combination of the two weighted with the event type fraction. Table VII presents the vertex efficiencies for 1VTX and 2VTX samples and their ratio.

TABLE VII: Vertex efficiencies for 1VTX and 2VTX samples and their ratio.

$\epsilon_{1vtx}$	$\epsilon_{2vtx}$	$\epsilon_{1vtx}/\epsilon_{2vtx}$
$0.944 \pm 0.003$	$0.922 \pm 0.003$	$1.021 \pm 0.005$

We also estimate the probability to lose a hard interaction event because no primary vertex is reconstructed. We find that the fraction of such events in the MB data sample with jet  $p_T > 15$  GeV is about 0.1% and about 0.2% for  $\gamma\gamma + \geq 1$  jet events in data. Due to the vertex reconstruction algorithm, we may also have an additional reconstructed vertex that passes the vertex requirement. Such a probability is estimated using  $\gamma\gamma + \geq 1$  jet events and  $\gamma\gamma + \geq 2$  jets events simulated in MC without ZB events overlaid (there should not be a second vertex in this case). The probability to have a second vertex is about 0.05%. Analogous estimates for dijet events (with requirement of  $\geq 1$  and  $\geq 2$  jets) gives about 0.1%.

#### E. Ratio of number of track efficiencies

For the DI fraction calculation, we use the CPF algorithm, described in Section VIB. The method requires  $\geq 2$  tracks and returns the highest CPF. The efficiency is calculated similarly to the vertex efficiency for each event type and then combined with the event type weights. Finally, the estimated number of DI events,  $N_{\text{DI}}$ , is corrected for the  $\epsilon_{N_{trk} \geq 2}$  efficiency which is found to be  $\epsilon_{N_{trk} \geq 2} = 0.725 \pm 0.004$ .

#### F. Calculating $R_c$ , $\sigma_{\text{hard}}$ , $N_1(c)$ and $N_2(c)$

We calculate the numbers of expected events with one ( $N_c(1)$ ) and two ( $N_c(2)$ )  $p\bar{p}$  collisions resulting in hard interactions following the procedure of Ref. [16], which uses the hard  $p\bar{p}$  interaction cross section  $\sigma_{\text{hard}} = 44.76 \pm 2.89$  mb. The values of  $N_c(1)$  and  $N_c(2)$  are obtained from a Poisson distribution parametrized with the average number of hard interactions in each bin of the instantaneous luminosity  $L_{\text{inst}}$  distribution,  $\langle n \rangle = (L_{\text{inst}}/f_{\text{cross}})\sigma_{\text{hard}}$ , where  $f_{\text{cross}}$  is the frequency of beam crossings for the Tevatron [26]. Summing over all  $L_{\text{inst}}$  bins, weighted with their fractions, we get  $R_c = (1/2)(N_c(1)/N_c(2))(\epsilon_{1vtx}/\epsilon_{2vtx}) = 0.45$ . This number is smaller by approximately a factor of two compared to that for the data collected earlier as reported in Ref. [16]. Since  $R_c$  and  $\sigma_{\text{hard}}$  enter Eq. 7 for  $\sigma_{\text{eff}}$  as a product, any increase of  $\sigma_{\text{hard}}$  leads to an increase of  $\langle n \rangle$  and, as a consequence, to a decrease in  $R_c$ , and vice versa. Due to this partial cancellation of uncertainties, although the measured value of  $\sigma_{\text{hard}}$  has a 6% relative uncertainty, the product  $R_c\sigma_{\text{hard}}$  only has a 2.6% uncertainty,  $R_c\sigma_{\text{hard}} = 18.92 \pm 0.49$  mb.

### VIII. RESULTS

We combine the results and use Eq. (7) to obtain  $\sigma_{\text{eff}}$ . The measured effective cross section with its total statistical and systematic uncertainty is given by Eq. (15). The main sources of systematic uncertainties are summarized in Table VIII. They are mostly caused by uncertainties in the DP and DI fractions, the ratio of efficiencies, acceptances in DP and DI events, and the ratio of photon fractions.

$$\sigma_{\text{eff}} = 21.3 \pm 1.5 \text{ (stat)} \pm 4.5 \text{ (syst)} \text{ mb} \quad (15)$$

TABLE VIII: Systematic and statistical uncertainties (in %). Total systematic uncertainty is caused by uncertainties on DP and DI fraction estimates, ratio of efficiencies and acceptances in DP and DI events, (“EffRatio”), ratio of photon fractions, (“Purity”), JES, and the uncertainty on the ratio of the number of events with single and double  $p\bar{p}$  hard collisions, (“ $R_c\sigma_{\text{hard}}$ ”).

$f_{DP}$	$f_{DI}$	EffRatio	Purity	JES	$R_c\sigma_{\text{hard}}$	SystTotal	StatTotal	Total
19.1	14.2	7.1	7.2	2.1	2.6	26.0	6.9	26.9

Figure 6 shows all the measurements of  $\sigma_{\text{eff}}$  performed by various experiments up to the present time. One can see that the  $\sigma_{\text{eff}}$  obtained by this measurement agrees with the recent  $D\bar{O}$  measurement [16] and with those obtained by other Tevatron and LHC experiments.

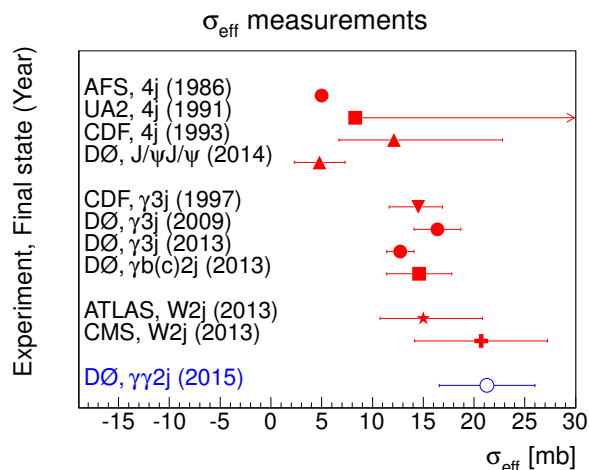


FIG. 6: (color online) Existing measurements of the effective cross section,  $\sigma_{\text{eff}}$ , compared to the result presented here (AFS: no uncertainty is reported; UA2: only a lower limit is provided).

### IX. SUMMARY

We have presented the measurement of fractions of double parton scattering processes  $f_{DP}$  in a single  $p\bar{p}$  collision with  $\gamma\gamma$ +dijet final states. In the chosen kinematical region with  $p_T^{\gamma_1} > 16$  GeV,  $p_T^{\gamma_2} > 15$  GeV,  $15 < p_T^{jets} < 40$  GeV, we observe  $19.3 \pm 3.7\%$  of events with double parton scattering in the  $\gamma\gamma$ +dijet final state. A parameter,  $\sigma_{\text{eff}}$ , characterizing the size of the interaction region in a nucleon is also measured and found to be  $\sigma_{\text{eff}} = 21.3 \pm 1.5 \text{ (stat)} \pm 5.7 \text{ (syst)}$  mb in the  $\gamma\gamma$ +dijet final state.

### Acknowledgements

We thank the staffs at Fermilab and collaborating institutions, and acknowledge support from the Department of Energy and National Science Foundation (United States of America); Alternative Energies and Atomic Energy Commission and National Center for Scientific Research/National Institute of Nuclear and Particle Physics (France); Ministry of Education and Science of the Russian Federation, National Research Center “Kurchatov Institute” of the Russian Federation, and Russian Foundation for Basic Research (Russia); National Council for the Development of Science and Technology and Carlos Chagas Filho Foundation for the Support of Research in the State of Rio de Janeiro (Brazil); Department of Atomic Energy and Department of Science and Technology (India); Administrative Department of Science, Technology and Innovation (Colombia); National Council of Science and Technology (Mexico); National Research Foundation of Korea (Korea); Foundation for Fundamental Research on Matter (The Netherlands); Science and Technology Facilities Council and The Royal Society (United Kingdom); Ministry of Education, Youth and Sports (Czech Republic); Bundesministerium für Bildung und Forschung (Federal Ministry of Education and Research) and Deutsche Forschungsgemeinschaft (German Research Foundation) (Germany); Science Foundation Ireland (Ireland); Swedish Research Council (Sweden); China Academy of Sciences and National Natural Science Foundation of China (China); and Ministry of Education and Science of Ukraine (Ukraine).

- 
- [1] P.V. Landshoff and J.C. Polkinghorne, *Calorimeter triggers for hard collisions*, Phys. Rev. D **18**, 3344 (1978); C. Goebel, F. Halzen, and D.M. Scott, *Double Drell-Yan annihilations in hadron collisions: Novel tests of the constituent picture*, Phys. Rev. D **22**, 2789 (1980).
  - [2] F. Takagi, *Multiple Production of Quark Jets off Nuclei*, Phys. Rev. Lett. **43**, 1296 (1979); N. Paver and D. Treleani, *Multiquark scattering and large- $p_T$  jet production in hadronic collisions*, Nuovo Cimento A **70**, 215 (1982).
  - [3] B. Humpert, *Are there multiquark interactions?*, Phys. Lett. B **131**, 461 (1983); B. Humpert and R. Odorico, *Multi-parton scattering and QCD radiation as sources of four-jet events*, Phys. Lett. B **154**, 211 (1985).
  - [4] T. Sjöstrand and M. van Zijl, *A multiple-interaction model for the event structure in hadron collisions*, Phys. Rev. D **36**, 2019 (1987).
  - [5] G. Calucci and D. Treleani, *Double parton scatterings in high-energy hadronic collisions*, Nucl. Phys. B (Proc. Suppl.) **71**, 392 (1999); G. Calucci and D. Treleani, *Proton structure in transverse space and the effective cross section*, Phys. Rev. D **60**, 054023 (1999).
  - [6] G. Calucci and D. Treleani, *Multiparton correlations and “exclusive” cross sections*, Phys. Rev. D **79**, 074013 (2009).
  - [7] C. Flensburg, G. Gustafson, L. Lonnblad, and A. Ster, *Correlations in double parton distributions at small  $x$* , J. High Energy Phys. 1106 (2011) 066.
  - [8] T. Sjöstrand and P. Z. Skands, *Multiple Interactions and the Structure of Beam Remnants*, J. High Energy Phys. 0403 (2004) 053.
  - [9] A. M. Snigirev, *QCD status of factorization ansatz for double parton distributions*, Phys. Rev. D **68**, 114012 (2003); V. L. Korotkikh and A. M. Snigirev, *Double parton correlations versus factorized distributions*, Phys. Lett. B **594**, 171 (2004).
  - [10] L. Frankfurt, M. Strikman, and C. Weiss, *Dijet production as a centrality trigger for  $p$ - $p$  collisions at CERN LHC*, Phys. Rev. D **69**, 114010 (2004); *Transverse nucleon structure and diagnostics of hard parton-parton processes at LHC*, Phys. Rev. D **83**, 054012 (2011).
  - [11] D. Bandurin, G. Golovanov, and N. Skachkov, *Double parton interactions as a background to associated  $H_W$  production at the Tevatron*, J. High Energy Phys. **1104**, 054 (2011).
  - [12] T. Akesson et al. (AFS Collaboration), *Double parton scattering in  $pp$  collisions at  $\sqrt{s} = 63$  GeV*, Z. Phys. C **34**, 163 (1987).
  - [13] J. Alitti et al. (UA2 Collaboration), *A study of multi-jet events at the CERN  $p\bar{p}$  collider and a search for double parton scattering*, Phys. Lett. B **268**, 145 (1991).
  - [14] F. Abe et al. (CDF Collaboration), *Study of four-jet events and evidence for double parton interactions in  $p\bar{p}$  collisions at  $\sqrt{s} = 1.8$  TeV*, Phys. Rev. D **47**, 4857 (1993).
  - [15] F. Abe et al. (CDF Collaboration), *Double parton scattering in  $p\bar{p}$  collisions at  $\sqrt{s} = 1.8$  TeV*, Phys. Rev. D **56**, 3811 (1997).
  - [16] V. M. Abazov et al. (D0 Collaboration), *Double parton interactions in  $\gamma + 3$  jet events in  $p\bar{p}$  collisions at  $\sqrt{s} = 1.96$  TeV*, Phys. Rev. D **81**, 052012 (2010).
  - [17] V. M. Abazov et al. (D0 Collaboration), *Azimuthal decorrelations and multiple parton interactions in  $\gamma + 2$  jet and  $\gamma + 3$  jet events in  $p\bar{p}$  collisions at  $\sqrt{s} = 1.96$  TeV*, Phys. Rev. D **83**, 052008 (2011).
  - [18] V. M. Abazov et al. (D0 Collaboration), *Double parton interactions in  $\gamma + 3$  jet and  $\gamma + b/c$ -jet + 2 jet events in  $p\bar{p}$  collisions at  $\sqrt{s} = 1.96$  TeV*, Phys. Rev. D **89**, 072006 (2014).
  - [19] V. M. Abazov et al. (D0 Collaboration), *Observation and studies of double  $J/\psi$  production at the Tevatron*, Phys. Rev. D **90**, 111101 (R) (2014).
  - [20] G. Aad et al. (ATLAS Collaboration), *Measurement of hard double-parton interactions in  $W(\rightarrow l\nu) + 2$ -jet events at  $\sqrt{s} = 7$  TeV with the ATLAS detector*, New J. Phys. **15**, 033038 (2013).
  - [21] S. Chatrchyan et al. (CMS Collaboration), *Study of double parton scattering using  $W + 2$ -jet events in proton-proton collisions at  $\sqrt{s} = 7$  TeV*, J. High Energy Phys., **1403** (2014).

- [22] The polar angle  $\theta$  and the azimuthal angle  $\phi$  are defined with respect to the positive  $z$  axis, which is along the proton beam direction. Pseudorapidity is defined as  $\eta = -\ln[\tan(\theta/2)]$ .  $\eta_{\text{det}}$  and  $\phi_{\text{det}}$  are the pseudorapidity and the azimuthal angle measured with respect to the center of the detector.
- [23] M. Drees and T. Han, *Signals for Double Parton Scattering at the Fermilab Tevatron*, Phys. Rev. Lett. **77**, 4142 (1996).
- [24] V. M. Abazov *et al.* (D0 Collaboration), *Hard Single Diffraction in  $p\bar{p}$  Collisions at  $\sqrt{s} = 630$  and  $1800$  GeV*, Phys. Lett. B **531**, 52 (2002);  
V. M. Abazov *et al.* (D0 Collaboration), *Observation of diffractively produced  $W$  and  $Z$  bosons in  $p\bar{p}$  collisions at  $\sqrt{s} = 1800$  GeV*, Phys. Lett. B **574**, 169 (2003).
- [25] V. M. Abazov *et al.* (D0 Collaboration), *Probing Hard Color-Singlet Exchange in  $p\bar{p}$  Collisions at  $\sqrt{s} = 630$  GeV and  $1800$  GeV*, Phys. Lett. B **440** 189 (1998).
- [26] V. M. Abazov *et al.* (D0 Collaboration), *The upgraded D0 detector*, Nucl. Instrum. Methods Phys. Res. A **565**, 463 (2006).
- [27] M. Abolins *et al.*, *Design and implementation of the new D0 level-1 calorimeter trigger*, Nucl. Instrum. Methods Phys. Res. A **584**, 75 (2008).
- [28] R. Angstadt *et al.*, *The layer 0 inner silicon detector of the D0 experiment*, Nucl. Instrum. Methods Phys. Res. A **622**, 298 (2010).
- [29] T. Andeen *et al.*, *The D0 Experiments Integrated Luminosity for Tevatron Run IIa*, FERMILAB-TM-2365, 2007.
- [30] V. M. Abazov *et al.* (D0 Collaboration), *Measurement of the differential cross section of photon plus jet production in  $p\bar{p}$  collisions at  $\sqrt{s} = 1.96$  TeV*, Phys. Rev. D **88**, 072008 (2013).
- [31] V. M. Abazov *et al.* (D0 Collaboration), *Electron and Photon Identification in the D0 Experiment*, Nucl. Instrum. Methods A **750**, 78 (2014).
- [32] V. M. Abazov *et al.* (D0 Collaboration), *Measurement of the differential cross sections for isolated direct photon pair production in  $p\bar{p}$  collisions at  $\sqrt{s} = 1.96$  TeV*, Phys. Lett. B **725**, 6 (2013).
- [33] G. C. Blazey *et al.*, *Run II Jet Physics: Proceedings of the Run II QCD and Weak Boson Physics Workshop*, arXiv:0005012 [hep-ex].
- [34] V. M. Abazov *et al.* (D0 Collaboration), *Jet energy scale determination in the D0 experiment*, Nucl. Instrum. Methods A **763**, 442 (2014).
- [35] T. Gleisberg *et al.*, *Event generation with Sherpa 1.1*, J. High Energy Phys. 02 (2009) 007.
- [36] T. Sjöstrand, *et al.*, *PYTHIA 6.4 Physics and Manual*, J. High Energy Phys. 05 (2006) 026.
- [37] R. Brun, F. Carminati, *CERN Program Library Long Writeup W5013*, (1993), unpublished.
- [38] R. Barlow and C. Beeston, *Fitting using finite Monte Carlo samples*, Comp. Phys. Comm. **77**, 219 (1993).
- [39] R. Hamberg, W. L. van Neerven, T. Matsuura, *A complete calculation of the order  $\alpha_s^2$  correction to the Drell-Yan  $K$ -factor*, Nucl. Phys. B **359**, 343 (1991) [Erratum-ibid. B **644**, 403 (2002)].